*ANZIAM J.* **62** (2020), 235–255
doi:10.1017/S144618112000022X

# CONFORMAL IMAGE REGISTRATION BASED ON CONSTRAINED OPTIMIZATION

S. MARSLAND[1], R. I. MCLACHLAN[2] and M. Y. TUFAIL[3]

(Received 25 July, 2019; accepted 16 September, 2020; first published online 12 January, 2021)

**Abstract**

Image registration is the process of finding an alignment between two or more images so that their appearances match. It has been widely studied and applied to several fields, including medical imaging and biology, where it is related to morphometrics. In this paper, we present a construction of conformal diffeomorphisms which is based on constrained optimization. We consider a set of different penalty terms that aim to enforce conformality, based on discretizations of the Cauchy–Riemann equations and geometric principles, and demonstrate them experimentally on a variety of images.

2020 *Mathematics subject classification*: primary 68U10; secondary 65E10.

*Keywords and phrases*: conformal diffeomorphisms, image registration, constrained optimization, numerical computation.

## 1. Introduction

Image registration is the process of finding an alignment between two or more images so that their appearances match. One of the key choices of image registration is the set of allowable transformations that can be used to deform the images. In this paper, methods of image registration using the set of conformal diffeomorphisms are derived and demonstrated. The motivation for the use of this group is the pioneering work of Thompson [26], who suggested that "simple" transformations that deformed an image of one animal to look like another could suggest evolutionary relationships between them.

Brown [5] gave a comprehensive review of image registration as it existed in 1992. The basic steps have not changed since; Brown suggests that they are (i) a

[1]School of Mathematics and Statistics, Victoria University of Wellington, Wellington, New Zealand; e-mail: stephen.marsland@vuw.ac.nz.
[2]School of Fundamental Sciences, Massey University, Palmerston North, New Zealand; e-mail: r.mclachlan@massey.ac.nz.
[3]Department of Mathematics, NED University of Engineering and Technology, Karachi, Pakistan; e-mail: tufail@neduet.edu.pk.

feature space (which contains information about the images), (ii) a search space (which consists of the set of allowable transformations), (iii) a search strategy (a way to select transformations to get an optimal solution), and (iv) a similarity metric (to measure the discrepancy between the images). However, the choice of possible transformations has certainly changed; Brown lists only three sets of transformations, all finite-dimensional: (a) affine transformations (rigid, shearing and aspect ratio, two-dimensional), (b) perspective transformations (of which projective transformations are special case) and (c) polynomial transformation, which can be used when less information is available about the camera geometry.

While there have been many developments in image registration since 1992 [9, 10, 24], the most significant change is the adoption of diffeomorphic (that is, smooth functions with smooth inverses) image registration [29]. The area where diffeomorphisms are most used in image registration is medical imaging, where images of parts of the human body from a variety of scanning methods, such as CT and MRI, are aligned either to assist in diagnosis of a disease, or to assist in surgical planning. This area is now known as *computational anatomy* [12, 27].

The most common approach of performing diffeomorphic registration is known as the *large deformation diffeomorphic metric mapping* (LDDMM) method [3, 15, 20].

The diffeomorphism group is infinite-dimensional, hence there may be many possible solutions to a matching between two images. However, it is a manifold as well as a group (although as an infinite-dimensional group, it is not a Lie group), which enables differential geometric methods to be applied in order to choose particular elements of the group, such as the geodesic between the representations of the two images (which is the source of the word *metric* in the LDDMM method). The metric on the diffeomorphism group can be used to identify images that are close together and, it is ultimately hoped, to perform statistical analysis of groups of images [8, 22, 25].

To date, diffeomorphic image registration has used the full group of diffeomorphisms. However, there are natural processes such as biological growth and evolution that seem to produce conformal deformations [23, 26, 27]. A possible biological explanation for this is that conformal deformations are locally rigid: linearization around any point yields a Euclidean similarity. In this paper we study conformal image registration.

**1.1. Image registration using a conformal diffeomorphism** Let $\Omega \subset \mathbb{R}^2$ be an image domain, and let $I_1, I_2 : \Omega \to \mathbb{R}$ be two greyscale images. We identify $\mathbb{R}^2$ with the standard complex plane $\mathbb{C}$ and write $z = x_1 + \mathrm{i}x_2$ for $(x_1, x_2) \in \mathbb{R}^2$. Let $\mathrm{con}(\Omega, \mathbb{C})$ be the set of maps $\hat{\varphi}$ that obey the following two properties: (i) $\hat{\varphi}(z)$ is complex analytic for all $z \in \Omega$; (ii) $\hat{\varphi}'(z) \neq 0$ for all $z \in \Omega$. These ensure that $\hat{\varphi}$ is conformal, invertible on its image, and has a conformal inverse. We define the objective function

$$E(\hat{\varphi}) = \int_\Omega ((I_1 \circ \hat{\varphi}^{-1})(x) - I_2(x))^2 \, dx_1 \, dx_2, \tag{1.1}$$

https://doi.org/10.1017/S144618112000022X Published online by Cambridge University Press

where $x = (x_1, x_2)^T$ and $\hat{\varphi} \in \mathrm{con}(\Omega, \mathbb{C})$. A process in which we find a $\hat{\varphi}$ that minimizes $E(\hat{\varphi})$ over $\hat{\varphi} \in \mathrm{con}(\Omega, \mathbb{C})$ is called a conformal image registration.

The issues that arise in image registration also turn up here. The two most significant challenges are: (i) the domain of $I_1 \circ \hat{\varphi}^{-1}$ is $\hat{\varphi}(\Omega)$, not $\Omega$, that is, the domains of the target and transformed source are not equal; (ii) the choice of an optimization algorithm. These are standard issues [19, 21, 29]. The new issue that arises in infinite-dimensional registration (that is, a registration which involves infinite-dimensional groups such as the full set of diffeomorphisms, the conformal group in this paper) is how to represent the diffeomorphisms. For diffeomorphic registration, this has been addressed in various ways [1, 3, 14, 17, 18]; this may in turn affect the optimization. Here we focus on how to represent the conformal maps.

The task of minimizing $E(\hat{\varphi})$ may be realized as a constrained optimization problem in which $E(\hat{\varphi})$ in equation (1.1) is defined for all invertible $\hat{\varphi}$, but we wish to find its minimum subject to the constraint that $\hat{\varphi}$ is conformal. We thus choose a penalty term and perform constrained optimization. This penalty term forces the diffeomorphism to be conformal. In other words, instead of using the objective function given in equation (1.1), we use the objective function

$$E(\varphi)_{\mathrm{con}} = \int_{\Omega} \{(I_1 \circ \varphi^{-1})(x) - I_2(x)\}^2 dx_1\, dx_2 + \lambda \int_{\Omega} P(y)^2\, dy_1\, dy_2. \tag{1.2}$$

Here $P(y)$, $y = (y_1, y_2)$, is a penalty term that vanishes if and only if $\varphi$ is a conformal diffeomorphism, that is, if and only if $\varphi$ satisfies the Cauchy–Riemann equations [11, 28] at the points $y$ and has nonzero derivative. Equation (1.2) is continuous and hence needs to be discretized to enable numerical computation, as is discussed next.

In Section 2 we present the discrete version of equation (1.2) for our control points method. Four penalty terms are derived and explained in Section 2. Implementation of control points method (with four penalty terms) on a variety of images is presented in Section 3. Section 4 discusses the conclusion of the research presented in this paper and our future research.

## 2. Control points method

In this section we present a discrete form of equation (1.2). First, we define the discrete domain $S$, the coordinates of the pixel locations. Typically these are arranged in an $N \times N$ square in $[-0.5, 0.5]^2$ leading to $N^2$ pixels at locations $x_{ij}$. In the control points method, the map $\varphi$ is represented by the values of $\varphi^{-1}$ on a *much coarser* grid than that of the discrete image domain $S$. Thus, we first choose $n^2$ grid points $\hat{x}_{ij}$ $(i, j = 1, \ldots, n)$ from the discrete domain $S$, where $n \ll N$, that are configured in an $n \times n$ grid. We then transform these chosen points under $\varphi^{-1}$ to generate another set of points of same size. We define two sets of points, the set of chosen points $\hat{x}_{ij} = \{\hat{x}_{11}, \hat{x}_{12}, \ldots, \hat{x}_{nn}\}$, and the set of transformed points $\hat{y}_{ij} = \{\hat{y}_{11}, \hat{y}_{12}, \ldots, \hat{y}_{nn}\}$ such that $\hat{y}_{ij} = \varphi^{-1}(\hat{x}_{ij})$. Here $\hat{x}_{ij} \in S$ and $\hat{y}_{ij} \in \mathbb{R}^2$. The variables $\hat{y}_{ij}$, which determine the map $\varphi$, are the dependent variables whose values will be determined during the optimization process. Larger

https://doi.org/10.1017/S144618112000022X Published online by Cambridge University Press

values of $n$ make the optimization process computationally much more expensive. The remaining values of $\varphi^{-1}$ that are needed to transform the source image, namely $\varphi^{-1}(x_{ij})$, are determined by bilinear interpolation from the known values $\varphi^{-1}(\hat{x}_{ij})$. The illustration of this approach with $n = 4$, that is, 16 control points and $N = 16$, that is, 256 grid points, is given in Figure 1.

The discrete form of equation (1.2) is now defined as

$$E(\varphi) = \sum_{i=1}^{N}\sum_{j=1}^{N}((I_1 \circ \varphi^{-1})(\hat{x}_{ij}) - I_2(\hat{x}_{ij}))^2 + \lambda \sum_{i=1}^{n}\sum_{j=1}^{n} P(\hat{y}_{ij})^2. \tag{2.1}$$

Equation (2.1) represents the general form of optimization function that will be used in this paper. It has two parts: the first part measures how well registered the images are, while the second part contains a penalty term $P$ related to the conformality of $\varphi$. The two terms are balanced by a parameter $\lambda$. We will see that for different choices of $P$ the second term may be either a constraint (in which case we will be interested in large values of $\lambda$ so that the constraint is satisfied, or nearly satisfied) or a regularization term, in which case $\lambda$ controls the trade-off between the quality of the registration and the conformality of $\varphi$.

The question is now how to choose the parameters. Our general approach is based on the continuation method, pioneered by Keller [16] and used here in a very simple form. The continuation parameters are $n$ and $\lambda$. For $\lambda$ there are two possible strategies to consider: (i) starting with a small or zero value of $\lambda$ and increasing it; and (ii) starting with a large or infinite value of $\lambda$ and decreasing it. In approach (i), if $\lambda = 0$, then the optimization problem reduces to the known problem of image registration, that is, the conformality condition has been dropped. In theory, this approach would first find the best registration with a diffeomorphism (which would necessarily be at least as good as the best registration with a conformal diffeomorphism), and then, by increasing $\lambda$, force it towards the best conformal registration. In approach (ii), if $\lambda$ is very large, we are initially enforcing the constraint or regularization term, which acts to better control the allowable transformations.

Depending on the choice of penalty term, it seems that both approaches could have some advantages and disadvantages. However, after conducting many numerical experiments, we settled on a uniform strategy of starting with large values of $\lambda$ (specifically, $\lambda = 20^4$) and decreasing it in steps of factors of 20. The problem is that if starting at $\lambda = 0$ the algorithm may fail to locate a smooth diffeomorphism registering the images even if we know (for example, because we are using synthetic data) that one exists.

In all the numerical experiments we have started with $n = 4$, that is, 16 control points, and minimized the objective function in equation (2.1) for $\lambda = 20^4, 20^3, 20^2$, 20, using the output of each optimization as the input for the next. We then set $n = 8$, that is, 64 control points, initializing the values for the new points by using bilinear interpolation from the $n = 4$ solution. Here $N = 100$ throughout. The approach is summarized in Algorithm 1.

https://doi.org/10.1017/S144618112000022X Published online by Cambridge University Press

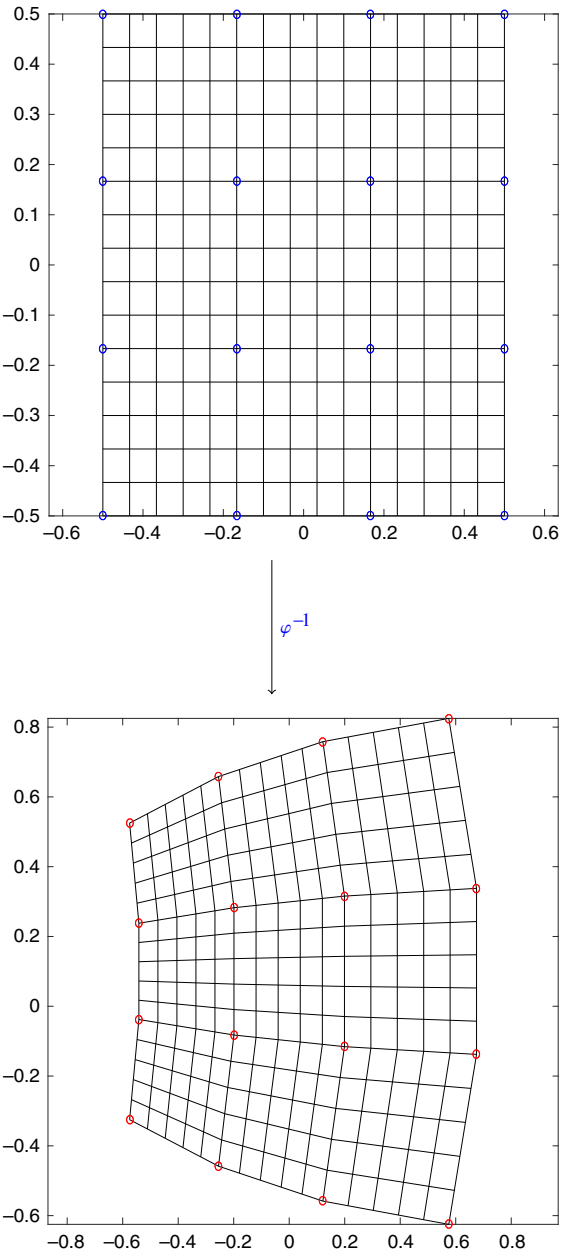


FIGURE 1. In the upper grid, the blue circles represent $n = 4$ selected control points from the discrete domain. In the lower grid, the images of the control points under $\varphi^{-1}$ are shown with red circles. Bilinear interpolation is used to generate the rest of the grid points between these red circles ($N = 16$). (See the online version of this paper for the colour scheme.)

https://doi.org/10.1017/S144618112000022X Published online by Cambridge University Press

The algorithm is not sensitive to the value of $N$. In principle, if sufficient computing power is available, then $N$ can be made very large. However, increasing the number of control points though $n$ is more problematic. As $n$ increases, the optimization step becomes more difficult and the conformal penalty term $P$ may not be sufficient to regularize the problem. This case deserves further study.

In the remainder of this paper we develop four alternative forms of the penalty term, that is, four alternative conceptions of a 'discrete conformal map', and test them using this algorithm. The performance of the algorithm may depend on the choice of the penalty term, whether we are using synthetic or real data (in synthetic data, the target is generated from the source using a known transformation, which may or may not be conformal), the smoothness of the images, the quality of the initial guess for the transformation, and how closely related the images are by a conformal map. Thus each form of the penalty term will be tested on a variety of images.

**Algorithm 1:** Image registration using control points and equation (2.1)

**input :** $I_1$ and $I_2$: source and target images
$N^2$: number of grid points
$n^2$: number of control points
$\hat{x}_{ij}$: selected control points from the discrete domain $S$
**output** Warp $\varphi^{-1}$ and deformed image $I_1 \circ \varphi^{-1}$
**:**
**for** $n = 4$ **do**
  initialize $\hat{y}_{ij}$ to $\hat{x}_{ij}$+ small random perturbation
  **for** $\lambda = 20^4, 20^3, 20^2, 20$*:* **do**
    optimize equation (2.1) to determine $\hat{y}_{ij} = \varphi^{-1}(\hat{x}_{ij})$
**for** $n = 8$ **do**
  **for** $\lambda = 20$ **do**
    $\hat{x}_{ij}$: initialize the values for the new points by using bilinear interpolation from the $n = 4$ solution.
    minimize equation (2.1) to determine $\hat{y}_{ij} = \varphi^{-1}(\hat{x}_{ij})$
    use bilinear interpolation to produce transformed grid, $y_{ij} = \varphi^{-1}(x_{ij}), \forall x_{ij} \in S$.
    use bilinear interpolation to obtain transformed version of the source, $I_1 \circ y_{ij}$.

PENALTY 1 (First discrete form of the Cauchy–Riemann equations). Our first discrete form is a naive finite difference of the Cauchy–Riemann equations at each of the $n^2$ control points. First we compute the numerical gradient and then determine the first form of the Cauchy–Riemann equations. Note that we identify $\mathbb{R}^2$ with the complex plane $\mathbb{C}$ as needed.

https://doi.org/10.1017/S144618112000022X Published online by Cambridge University Press

We calculate the gradient of $\hat{y}_{ij}$ using central differences at the interior points,

$$(\Delta_x \hat{y})_{i,j} = (\hat{y}_{i+1,j} - \hat{y}_{i-1,j})/2, \quad i = 2, 3, \ldots, n-1, \tag{2.2}$$

$$(\Delta_y \hat{y})_{i,j} = (\hat{y}_{i,j+1} - \hat{y}_{i,j-1})/2, \quad j = 2, 3, \ldots, n-1, \tag{2.3}$$

and one-sided differences at edge points,

$$(\Delta_x \hat{y})_{1,j} = \hat{y}_{2,j} - \hat{y}_{1,j}, \quad (\Delta_x \hat{y})_{n,j} = \hat{y}_{n,j} - \hat{y}_{n-1,j}, \tag{2.4}$$

$$(\Delta_y \hat{y})_{i,1} = \hat{y}_{i,2} - \hat{y}_{i,1}, \quad (\Delta_y \hat{y})_{i,n} = \hat{y}_{i,n-1} - \hat{y}_{i,n}. \tag{2.5}$$

Identifying $\hat{y}$ with $\varphi$, the first discrete form of the Cauchy–Riemann equations that we use is

$$\Delta_x \hat{y}_{ij} = -\mathrm{i}\Delta_y \hat{y}_{ij}, \quad i, j = 1, \ldots, n. \tag{2.6}$$

Note that we are using here the fact that the reference grid of control points, $\hat{x}_{ij}$, is a uniform square grid, as we use such a grid in all our experiments. The mesh size of this grid has been effectively absorbed into the parameter $\lambda$. This discrete form of the Cauchy–Riemann equation is used to define our Penalty 1 as

$$P_1(\hat{y}_{ij}) = |(\Delta_x \hat{y}_{ij} + \mathrm{i}\Delta_y \hat{y}_{ij})|. \tag{2.7}$$

We found in our numerical experiments (not reported in this paper) that when $\lambda \to \infty$, $\|P_1(\hat{y})\| \to 0$ and that the discrete maps produced in this way were always rigid transformations, that is, Euclidean similarities [2, 7]. ♠

PENALTY 2 (Second discrete form of the Cauchy–Riemann equations). We consider the linear discrete form of the Cauchy–Riemann equations introduced by Bobenko et al. [4].

Penalty 2 is based on the *linear discrete Cauchy–Riemann equations* [4]:

$$\varphi_{m,n+1} - \varphi_{m+1,n} = \mathrm{i}(\varphi_{m+1,n+1} - \varphi_{m,n}). \tag{2.8}$$

This compact finite difference is a second order discretization of the Cauchy–Riemann equations. On a square cell centre 0 and side $2h$, equation (2.8) yields

$$(\varphi(-h, h) - \varphi(h, -h)) = \mathrm{i}(\varphi(h, h) - \varphi(-h, -h)). \tag{2.9}$$

Taylor series expansion at $(0, 0)$ yields

$$(-2h\varphi_x + 2h\varphi_y) - \mathrm{i}(2h\varphi_x + 2h\varphi_y) = O(h^3) \tag{2.10}$$

or

$$(\varphi_x + \mathrm{i}\varphi_y)(-1 - \mathrm{i}) = O(h^2). \tag{2.11}$$

That is, if $\varphi(z)$ satisfies the Cauchy–Riemann equations then it satisfies the linear discrete Cauchy–Riemann equations with a discretization error of $O(h^2)$.

https://doi.org/10.1017/S144618112000022X Published online by Cambridge University Press

We therefore define our second penalty term, based on the linear discrete Cauchy–Riemann equations, as

$$P_2(\hat{y}_{ij}) = |(\hat{y}_{i,j+1} - \hat{y}_{i+1,j}) - \mathrm{i}(\hat{y}_{i+1,j+1} - \hat{y}_{i,j})|, \quad i,j = 1,\ldots,n-1. \tag{2.12}$$

♠

PENALTY 3 (Third discrete form of the Cauchy–Riemann equations). Penalty 3 is based on the *nonlinear discrete Cauchy-Riemann equations* [4]:

$$\frac{(\varphi_{m+1,n} - \varphi_{m,n})(\varphi_{m+1,n+1} - \varphi_{m,n+1})}{(\varphi_{m,n+1} - \varphi_{m,n})(\varphi_{m+1,n+1} - \varphi_{m+1,n})} = -1. \tag{2.13}$$

We now show that this form is also a second order discretization of the Cauchy–Riemann equations. Equation (2.13) for a square is

$$\frac{(\varphi(h,-h) - \varphi(-h,-h))(\varphi(h,h) - \varphi(-h,h))}{(\varphi(-h,h) - \varphi(-h,-h))(\varphi(h,h) - \varphi(h,-h))} = -1. \tag{2.14}$$

Rearranging equation (2.14),

$$\begin{aligned}&\{\varphi(h,-h) - \varphi(-h,-h)\}\{\varphi(h,h) - \varphi(-h,h)\}\\ &\quad + \{\varphi(-h,h) - \varphi(-h,-h)\}\{\varphi(h,h) - \varphi(h,-h)\} = 0.\end{aligned} \tag{2.15}$$

Expanding equation (2.15) in Taylor series about (0,0) gives

$$(\varphi_x + \mathrm{i}\varphi_y)(\varphi_x - \mathrm{i}\varphi_y) = O(h^2). \tag{2.16}$$

Therefore, if $\varphi(z)$ is either conformal or anticonformal (a conformal map of $\bar{z}$, that is, a composition of a reflection and a conformal map) then it will satisfy the nonlinear discrete Cauchy–Riemann equations with a discretization error of $O(h^2)$. Thus, the third penalty term is defined as

$$P_3(\hat{y}_{ij}) = |(\hat{y}_{i+1,j} - \hat{y}_{i,j})(\hat{y}_{i+1,j+1} - \hat{y}_{i,j+1}) + (\hat{y}_{i,j+1} - \hat{y}_{i,j})(\hat{y}_{i+1,j+1} - \hat{y}_{i+1,j})|, \quad i,j = 1,\ldots,n-1. \tag{2.17}$$

♠

The linear form (Penalty 2) is based on the cross-ratio, whereas the nonlinear form (Penalty 3) is based on the notion of a circle pattern. They both have strong theoretical reasons to be considered as natural discrete analogues of conformality, including applications to integrability.

It is possible that, when using the Penalty 3, the penalty term could be zero and the grid would approximate an anticonformal map instead of a conformal map. However, this has not happened in any of our experiments, but it is a difference between Penalty 2 and Penalty 3.

Penalty 2 ($P_2(\hat{y}_{ij})$ in equation (2.12)) and Penalty 3 ($P_3(\hat{y}_{ij})$ in equation (2.17)) are less restrictive than Penalty 1 ($P_1(\hat{y}_{ij})$ in equation (2.7)). This is because they contain fewer equations (one per cell instead of one per grid point), and they can be satisfied

https://doi.org/10.1017/S144618112000022X Published online by Cambridge University Press

by many nonrigid mappings. A discrete mapping is determined by $2n^2$ real parameters, while the equations $P_2(\hat{y}_{ij}) = 0$ for $i, j = 1, \ldots, n-1$ (respectively, $P_3$) require $2(n-1)^2$ equations. Thus we expect there to be $2n^2 - 2(n-1)^2 = 4n - 2$ free parameters in their solution.

Note that the counting of these discrete forms is different from that of the continuous Cauchy–Riemann equations. For the continuous form, the real part of $\varphi$ can be specified on the boundary and its values in the interior determined by solving Laplace's equation $\nabla^2(\Re(\varphi)) = 0$ which has a unique solution. The imaginary part of $\varphi$ is then determined up to a constant. But in the discrete case, once the real part of $\hat{y}_{ij}$ is specified on the boundary (that is, $4n - 4$ conditions imposed), there remain two degrees of freedom (not one) for the imaginary part.

Also note that there are discrete maps satisfying $P_2 = 0$ or $P_3 = 0$ which contain "butterflies" in which the edges of the image quadrilateral intersect. The resulting continuous map obtained by bilinear interpolation would not then be invertible (see Examples 2 and 3 in Section 3). In fact, the poor results of the first three penalty terms $(P_1(\hat{y}_{ij}), P_2(\hat{y}_{ij}), P_3(\hat{y}_{ij})$ in equations (2.7), (2.12) and (2.17), respectively) on some registration problems motivated us to introduce a fourth penalty term, explained below.

PENALTY 4 (Fourth form of the penalty term). Let $\varphi\colon \Omega \to \mathbb{C}$ be a conformal map. The following equation indicates expanding about any point $z_0 \in \Omega$ in Taylor series as

$$\varphi(z) = \varphi(z_0) + (z - z_0)\varphi'(z_0) + O(|z - z_0|^2). \tag{2.18}$$

Thus, conformal maps are local similarities in the neighbourhood of any point. Therefore, small squares map to squares, with an error that vanishes as the square becomes smaller. Therefore, we use this geometric property of the conformal transformation to compute our fourth penalty term.

Consider a square in Figure 2 whose sides are $a$, $b$, $c$, $d$, respectively, considered as displacement vectors in the complex plane (equivalently, as complex numbers) taken in an anticlockwise sense. The following equations holds for a square:

$$\begin{cases} a + \mathrm{i}b = 0, \\ b + \mathrm{i}c = 0, \\ c + \mathrm{i}d = 0, \\ d + \mathrm{i}a = 0. \end{cases} \tag{2.19}$$

This leads us to define our fourth penalty term

$$P_4(\hat{y}_{ij}) = \frac{(a + \mathrm{i}b, b + \mathrm{i}c, c + \mathrm{i}d, d + \mathrm{i}a)}{|(a, b, c, d)|} \tag{2.20}$$

for $i, j = 1, \ldots, n-1$. Here $a$, $b$, $c$, and $d$ are the vectors of the sides of the quadrilateral with vertices $\hat{y}_{i,j}$, $\hat{y}_{i+1,j}$, $\hat{y}_{i+1,j+1}$, and $\hat{y}_{i,j+1}$ and $(a, b, c, d)$ is the cross-ratio. Thus the fourth penalty term in equation (2.20) contains four complex or eight real

https://doi.org/10.1017/S144618112000022X Published online by Cambridge University Press

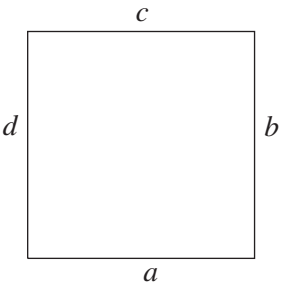


FIGURE 2. A square with four displacement vectors, $a$, $b$, $c$ and $d$, in the complex plane with anticlockwise orientation.

terms per cell. There are $(n-1)^2$ cells, so the penalty contains $8(n-1)^2$ real terms altogether. ♠

The motivation for regarding $P_4$ (equation (2.20)) as a discrete version of conformality is that:

- when $P_4$ is small, squares map to approximate squares;
- it is invariant under translation, rotation, scaling, and cyclic permutations of the vertices;
- each term (for example, $a + \mathrm{i}b$) is a first-order finite difference of the Cauchy–Riemann equations at one vertex;
- linear combinations of the conditions at adjacent cells give the standard central difference discretization of the Cauchy–Riemann equations used in the first penalty term.

Like $P_2$ and $P_3$ it is associated with the cells, rather than the control points like $P_1$, but compared to $P_1$, $P_2$ and $P_3$ it controls far more terms. Note that for any quadrilateral, $a$, $b$ and $c$ together determine $d$, so only six of the eight real terms are independent.

If $P_4(\hat{y}_{ij}) = 0$ for all $i,j = 1,\ldots,n-1$, then the transformation determined by the $\hat{y}_{ij}$ is rigid. So $P_4$ is like $P_1$ in this regard. Therefore $\lambda \to \infty$ will yield only rigid transformations, and we again regard $\lambda$ as a regularization parameter, offering the opportunity for parameter continuation between $\lambda = 0$ (unconstrained image registration), moderate $\lambda$ (squares map to near squares), and large $\lambda$ (rigid registration).

As we will be minimizing the sum of the registration error plus $\lambda$ times $\|P_4\|^2$, the solutions will map squares to near squares only in an average sense; some squares may suffer extreme distortion. In view of the difficulties faced by our first three penalty terms, we argue that the extra flexibility this allows will be needed. A possible topic for future research would be to replace $P_4$ by related functions (such as $P_4^\alpha$ for $\alpha > 1$) that penalize nonsquareness more severely.

https://doi.org/10.1017/S144618112000022X Published online by Cambridge University Press

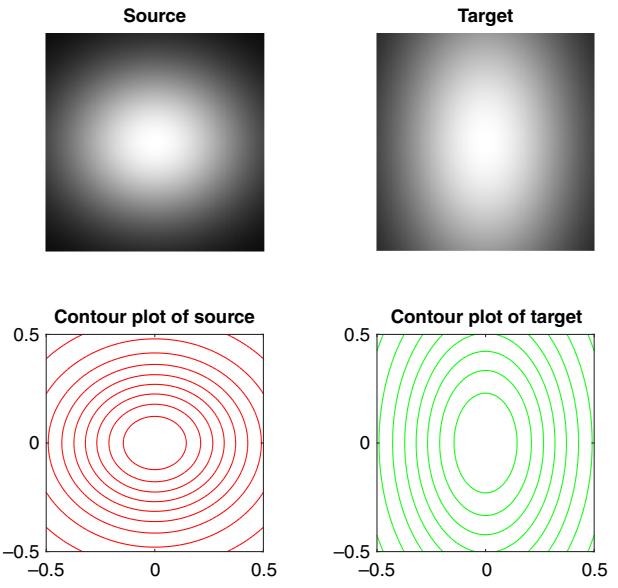


FIGURE 3. The source and target images for Example 1. The source is $\exp(-5x^2 - 7y^2)$, the target is $\exp(-5x^2 - 2y^2)$. The corresponding contour plots can be seen in the second row. (Colour available online.)

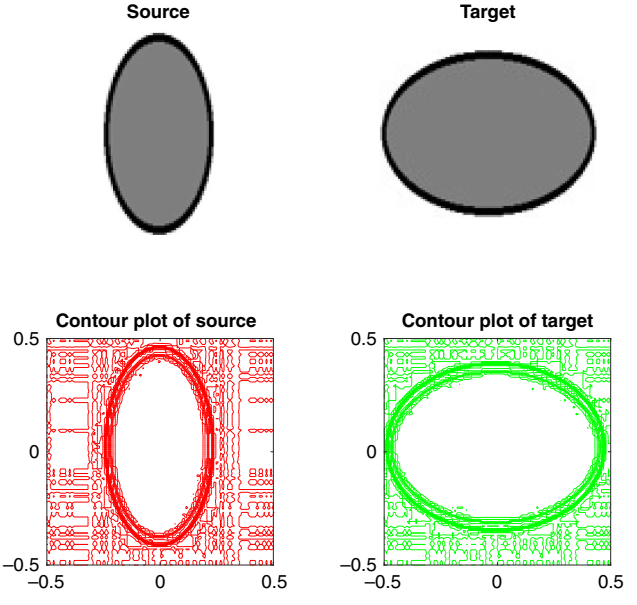


FIGURE 4. The two nonsmooth images of ellipses used as the source and target in Example 2. (Colour available online.)

https://doi.org/10.1017/S144618112000022X Published online by Cambridge University Press

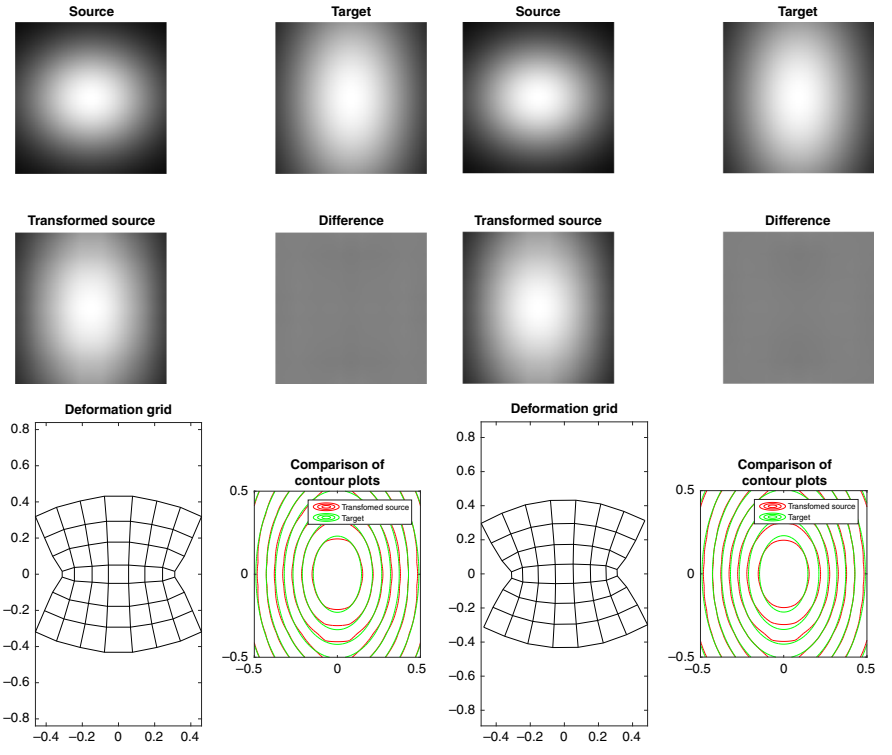


(a) Result of Penalty 1 (b) Result of Penalty 2

FIGURE 5. Implementation of Algorithm 1 produced two sets of conformal image registrations using two penalty terms. Top: Results for Penalty 1 and Penalty 2 (from left to right). Bottom: Comparison of contour plots and corresponding deformation grids for Penalty 1 and Penalty 2 (from left to right). The conformality parameters $\lambda$ is 20 for each penalty. (Colour available online.)

## 3. Experiments

In this section we present the results of applying each of the four discrete conformal penalty terms to three examples: (1) a pair of smooth images that are nearly conformally related; (2) a pair of nonsmooth images that are nearly conformally related; (3) a pair of nonsmooth images that are not known to be conformally related. In all examples, the domain is $\Omega = [-0.5, 0.5]^2$ and $N = 100$.

EXAMPLE 1. In this example we take a pair of smooth images, $I_1 = \exp(-5x^2 - 7y^2)$ and $I_2 = \exp(-5x^2 - 2y^2)$. The level sets of each are ellipses (see Figure 3). By the Riemann mapping theorem, any ellipse can be mapped conformally to any other ellipse, although the images themselves are not conformally related. As shown in Figures 5 and 6, all four penalty forms produce a smooth transformation and a good registration, although there are some differences. The registration errors for the four penalties are 0.92, 1.09, 0.16, and 1.41, respectively. Penalty term 3 has produced the

https://doi.org/10.1017/S144618112000022X Published online by Cambridge University Press

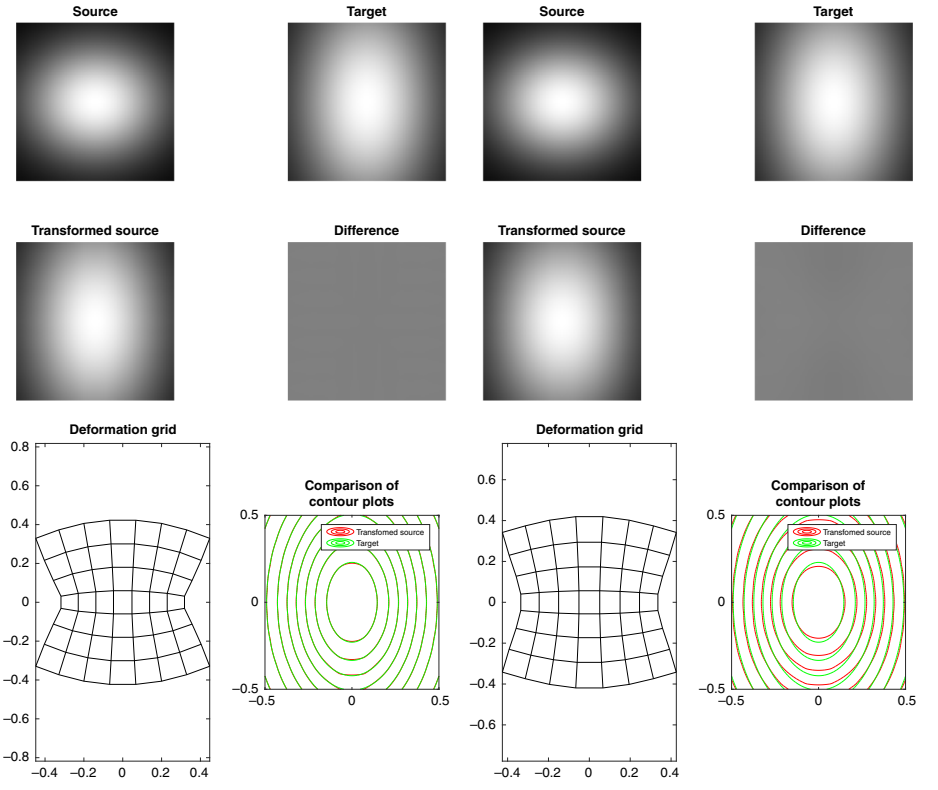


(a) Result of Penalty 3 (b) Result of Penalty 4

FIGURE 6. Implementation of Algorithm 1 produced two sets of conformal image registrations using two penalty terms. Top: Results for Penalty 3 and Penalty 4 (from left to right). Bottom: Comparison of contour plots and corresponding deformation grids for Penalty 3 and Penalty 4 (from left to right). The conformality parameters $\lambda$ for the Penalty 3 and Penalty 4 are 20 and 150, respectively. (Colour available online.)

best registration (that is, the minimum error), with a mean error of just 0.0016 per pixel (on a scale of $[0, 1]$). In other tests (not shown), we have confirmed that all four penalties can produce a good registration and a smooth transformation, when the images are smooth and are related by a smooth conformal map.

EXAMPLE 2. In this example the images are nonsmooth, but are known (from the Riemann mapping theorem) to be very nearly conformally related. We take drawings of two different ellipses (see Figure 4). The boundaries are drawn with thick black lines to penalize any mismatch of the boundaries. The results are shown in Figures 7 and 8. The black region (here and elsewhere) in the transformed source indicates the set of points that have no colour information (missing values). These missing values are dealt with by appropriate scaling (see [28, Ch.3]). Penalty 1 produces an acceptable solution, although the mapping is less smooth than necessary. This is clearly visible

https://doi.org/10.1017/S144618112000022X Published online by Cambridge University Press

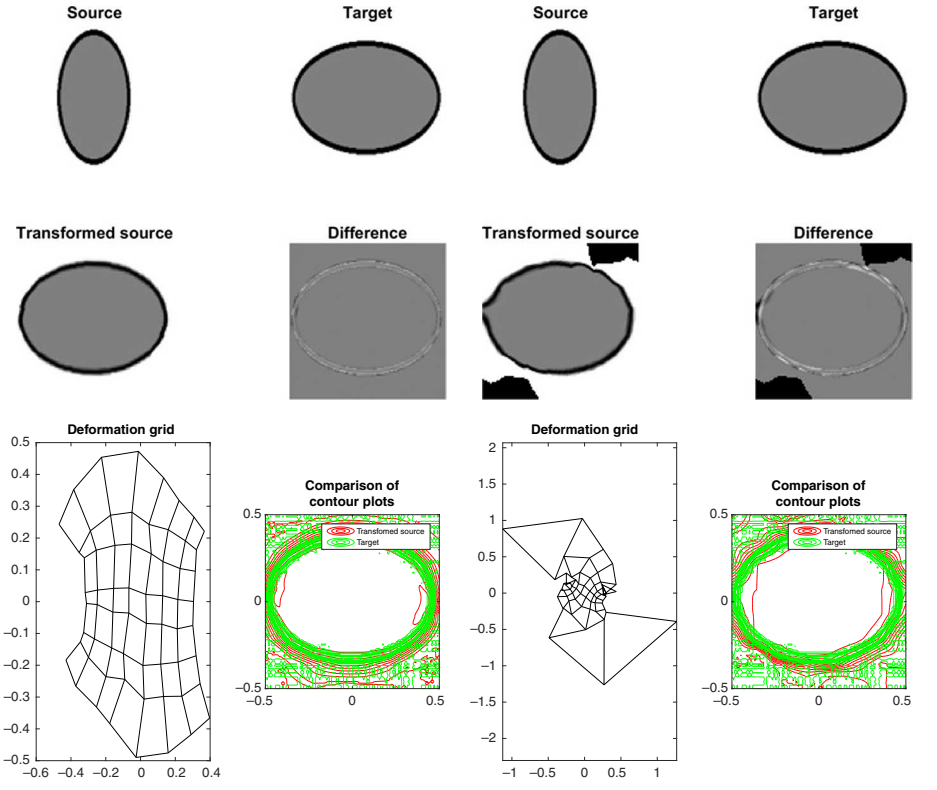


(a) Result of Penalty 1 (b) Result of Penalty 2

FIGURE 7. The source and target are filled drawings of ellipses of different aspect ratios. Some small textural differences between the two images can be seen in the background of the images. This is an interpolation artefact caused by the interpolation of the images onto the $100 \times 100$ pixel grid. Top: Registration results for Penalty 1 and Penalty 2. Bottom: Comparison of contour plots along with deformation grids for Penalty 1 and Penalty 2. The conformality parameters $\lambda$ is 20 for first two penalty terms. (Colour available online.)

in the transformed source. Penalty 2 produces a very irregular mapping that fails to be invertible in two places. (The huge deformations outside the domain can be ignored; as there are no overlapping parts of the images here, the values of $\hat{y}_{ij}$ are constrained only by the discrete conformality constraint, not the images.) In Penalty 3, the transformed source is smoother, but the mapping is very poor, failing to be invertible in many places. Penalty 4 produces a good registration and a smooth, invertible mapping. (Note that the optimization process has found a solution that includes a rotation by 90°; the top of the source has mapped to the left of the target.) The registration errors for the four penalties are 4.62, 8.51, 3.94, and 5.73, respectively.

EXAMPLE 3. This example involves source and target images that are nonsmooth and are presumed not to be nearly conformally related. The example is inspired

https://doi.org/10.1017/S144618112000022X Published online by Cambridge University Press

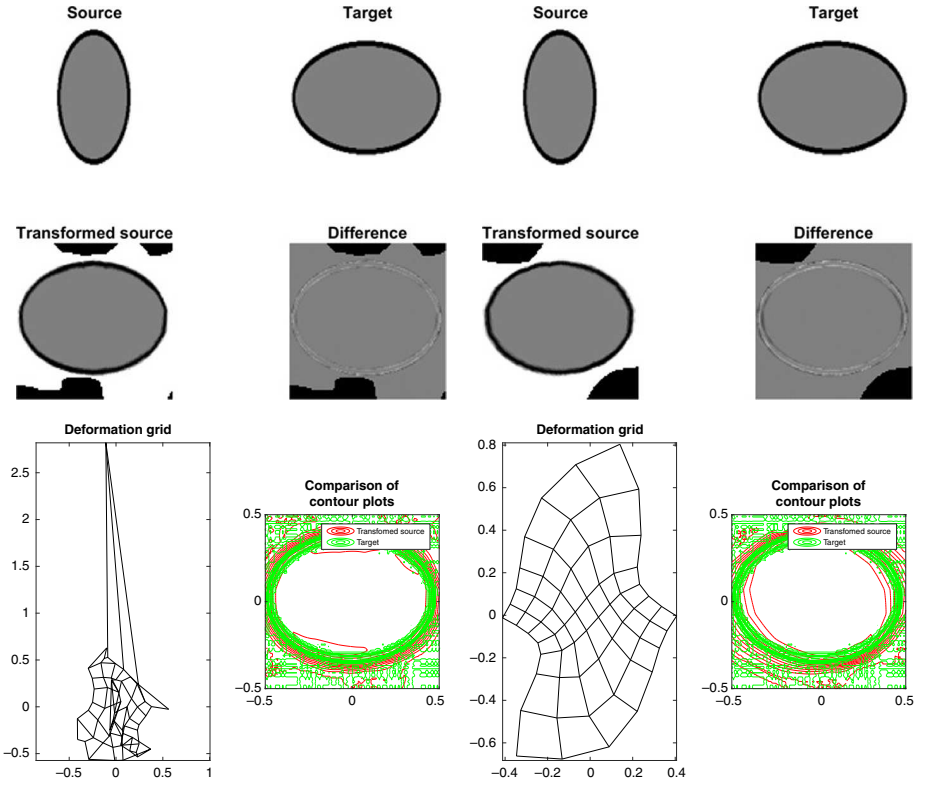


(a) Result of Penalty 3 (b) Result of Penalty 4

FIGURE 8. Implementation of Algorithm 1 for Example 2 using Penalty 3 and Penalty 4. Top: Registration results for Penalty 3 and Penalty 4 (left to right). Bottom: Deformation grid and contour plots for Penalty 3 and Penalty 4, respectively. The conformality parameters $\lambda$ for Penalty 3 and Penalty 4 are 20 and 150, respectively. (Colour available online.)

by one of Thompson's nonrigid registrations of fish [27]. Indeed, Thompson, in an informal model-selection procedure, tended to select transformations from the simplest set that gave what was, to him, an acceptable registration. Where affine, projective or axis-preserving transformations would not do the job, he was forced to use more highly nonlinear mappings and choose a conformal map (unless forced by the images not to do so). He wrote: "It is true that, in a mathematical sense, it is not a perfectly satisfactory, or perfectly regular, deformation, for the system is no longer orthogonal; but nevertheless it is symmetrical to the eye, and obviously approaches to an orthogonal system under certain conditions of friction or lateral constraint." The cartoon images of fish used in this example are shown in Figure 9 and the results in Figures 10 and 11. Although in all four penalties the optimizer has managed to broadly overlap the fish bodies, in Penalties 1, 2 and 3 the transformations are wildly irregular and noninvertible. In striking contrast, Penalty 4 has produced an acceptable

https://doi.org/10.1017/S144618112000022X Published online by Cambridge University Press

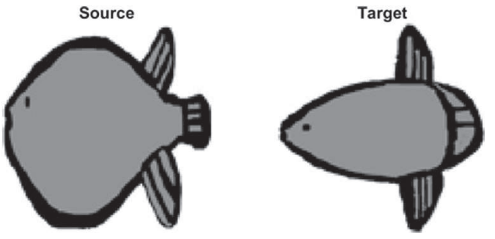


FIGURE 9. The two nonsmooth cartoon fish images used in Example 3. The images are presumed not to be closely conformally related.

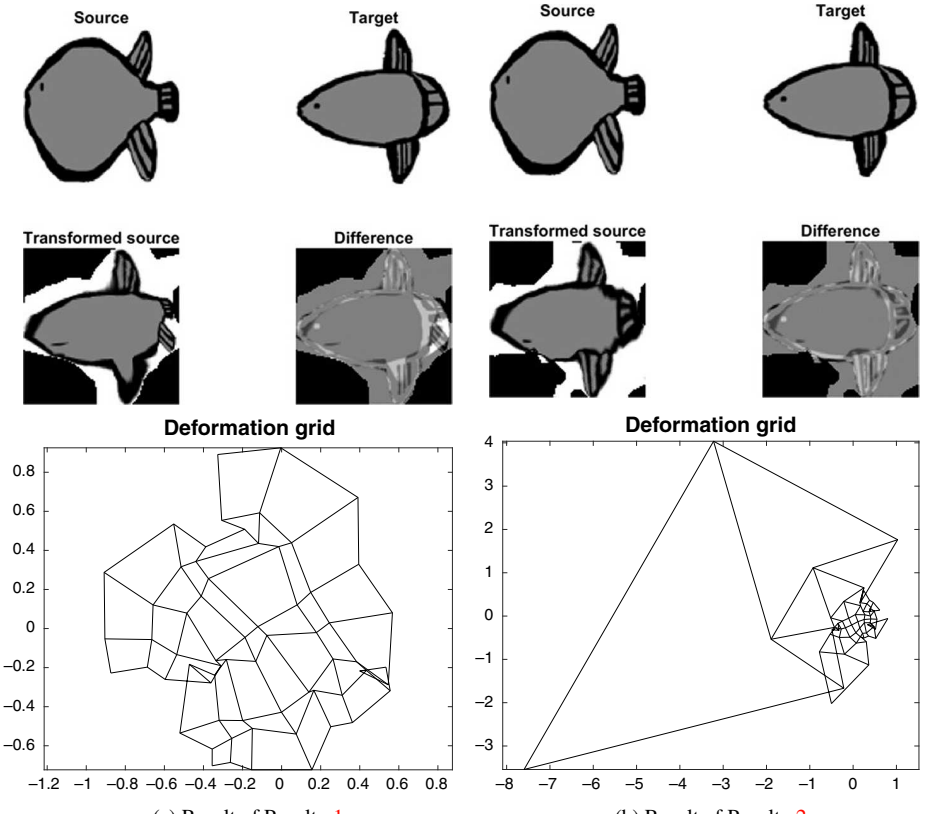


(a) Result of Penalty 1 (b) Result of Penalty 2

FIGURE 10. Implementation of Algorithm 1 over pair of non-smooth images with non-synthetic data using Penalty 1 and Penalty 2. Top: Registration results for Penalty 1 and Penalty 2 (left to right). Bottom: Respective deformation grids. The conformality parameter $\lambda$ is set as 20 for Penalty 1 and Penalty 2.

https://doi.org/10.1017/S144618112000022X Published online by Cambridge University Press

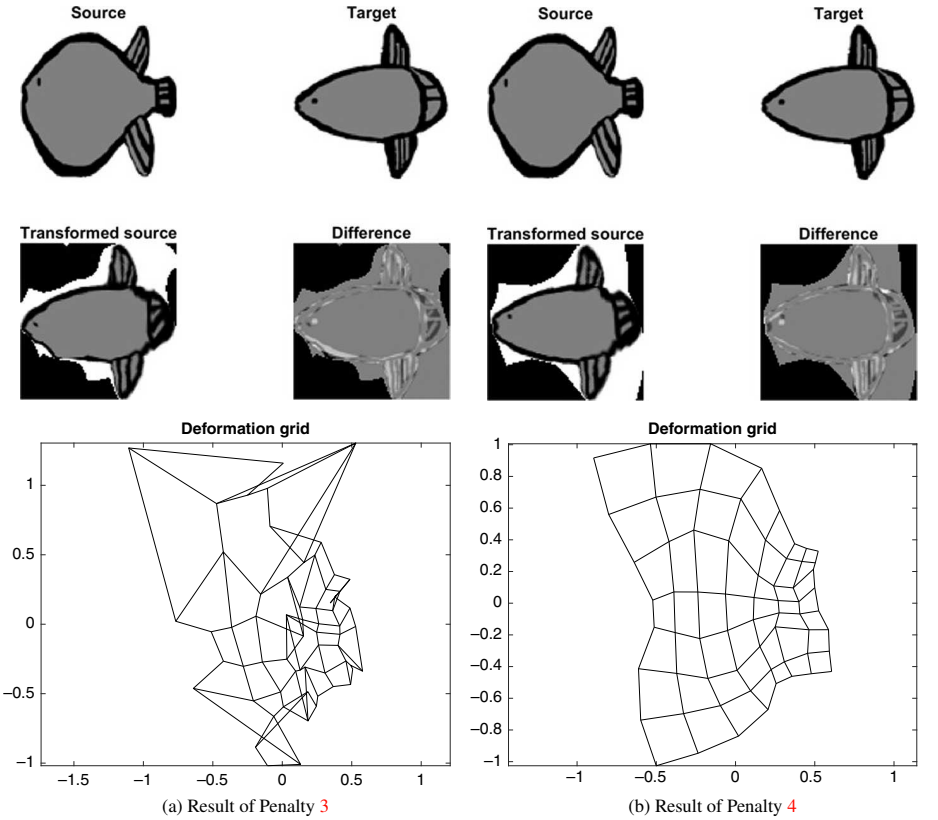


(a) Result of Penalty 3 (b) Result of Penalty 4

FIGURE 11. Implementation of Algorithm 1 on a pair of nonsmooth images with nonsynthetic data. Top: Registration results for Penalty 3 and Penalty 4. Bottom: Deformation grids for Penalty 3 and Penalty 4, respectively. The conformality parameters $\lambda$ for the Penalty 3 and Penalty 4 are 20 and 150, respectively.

registration with an invertible (and fairly smooth) mapping. The registration errors are 19.00, 15.37, 13.77 and 13.19, respectively.

As Penalty 4 looks promising we present further results in Figure 12, which shows the registration results for six different $\lambda$ values selected from the continuation process. The graph of registration error against $1/\lambda$ shows a classic L-curve [6] widely seen in (for example, Tikhonov [13]) regularization in inverse problems: the usual prescription there is to choose $\lambda$ near the corner of the L-curve (although this is coordinate-dependent). The registrations begin to deteriorate markedly only for $\lambda \gtrsim 300$; beyond this point the transformation is constrained to become more and more nearly rigid, tending to a Euclidean similarity. The best trade-off between a better registration and a more nearly conformal mapping is not one that can be determined definitively. What is striking is that the transformations that are produced are invertible and are fairly regular with few highly distorted cells, even for the smallest value of $\lambda$ considered. This is in marked contrast to the other penalties.

https://doi.org/10.1017/S144618112000022X Published online by Cambridge University Press

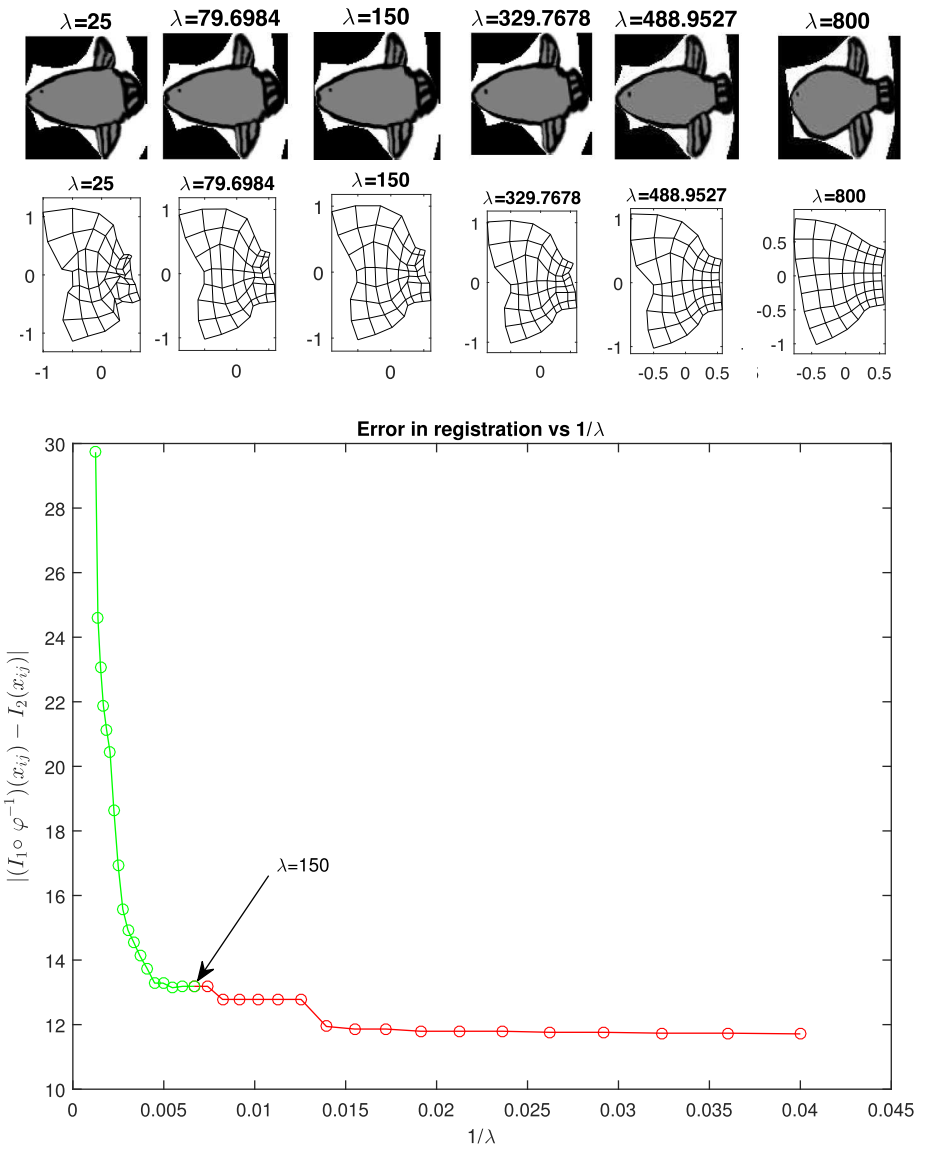


FIGURE 12. Effect of conformality parameter $\lambda$ on registration for Example 3, discrete conformal Penalty 4. As $\lambda \to \infty$, the transformation tends to a Euclidean similarity. At $\lambda = 0$, conformality is ignored and we are simply fitting an arbitrary piecewise bilinear transformation. *Top*: The transformed sources (which can be compared to the target shown in Figure 9 and the grid transformations. *Bottom*: The registration error plotted against $1/\lambda$, showing a classic regularization L-curve. (Colour available online.)

https://doi.org/10.1017/S144618112000022X Published online by Cambridge University Press

## 4. Conclusions

All four discrete conformality conditions can produce acceptable results in some conditions, especially if the images are smooth and nearly conformally related. Numerical experiments (including others not shown here) have convinced us that Penalties 1, 2, and 3 are not sufficiently robust for this application, but that Penalty 4 shows promise and deserves further consideration as a criterion of discrete conformality, both in the present conformal image registration problem and elsewhere.

Penalties 2 and 3, based on known discrete conformality conditions with many appealing theoretical properties, do not perform well for conformal registration. The mappings are not invertible. The discrete conformality condition under-constrains the mappings, even at $\lambda = \infty$. It would be difficult to constrain them to be invertible as this is an open condition (that is, it would produce mappings that almost fail to be invertible), while adding further regularization based on, for example, $\| \det D\varphi \|$ (which blows up as $\varphi^{-1}$ approaches noninvertibility) is possible, but would compete with the conformality.

Penalty 1, which like Penalty 4 is over-constrained and produces transformations that tend to Euclidean similarities as $\lambda \to \infty$, also performs poorly. It is more sensitive to the precise value of $\lambda$ (not shown). and does not produce good transformations and registrations over a wide range of $\lambda$ values. Thus our investigation suggests that both Penalty 1 and Penalty 4 produce poor transformations and registrations over a wide range of $\lambda$ values.

We do not have a full understanding of the implications of the discrete conformality condition presented in Penalty 4, equation (2.20). Based on its geometric origin, its symmetries, its connection to finite differences of the Cauchy–Riemann equation, and its good performance in conformal image registration, it warrants further attention.

## Acknowledgement

This research was supported by the Royal Society of New Zealand Marsden Fund, Te Apārangi.

## References

[1] V. Arsigny, O. Commowick, N. Ayache and X. Pennec, "A fast and log-Euclidean polyaffine framework for locally linear registration", *J. Math. Imaging Vis.* **33** (2009) 222–238; doi:10.1007/s10851-008-0135-9.

[2] J. Ashburner and K. J. Friston, "Rigid body registration", in: *Statistical parametric mapping: the analysis of functional brain images* (eds. W. Penny, K. Friston, J. Ashburner, S. Kiebel and T. Nichols), (Elsevier, Amsterdam, 2007) 49–62; doi:10.1016/b978-012372560-8/50004-8.

[3] M. F. Beg, M. I. Miller, A. Trouvé and L. Younes, "Computing large deformation metric mappings via geodesic flows of diffeomorphisms", *Int. J. Comput. Vis.* **61** (2005) 139–157; doi:10.1023/b:visi.0000043755.93987.aa.

[4] A. I. Bobenko, C. Mercat and Y. B. Suris, "Linear and nonlinear theories of discrete analytic functions. Integrable structure and isomonodromic Green's function", *J Reine Angew. Math.* **583** (2005) 117–161; doi:10.1515/crll.2005.2005.583.117.

[5] L. G. Brown, "A survey of image registration techniques", *ACM Comput. Surv.* **24** (1992) 325–376; doi:10.1145/146370.146374.
[6] D. Calvetti, S. Morigi, L. Reichel and F. Sgallari, "Tikhonov regularization and the l-curve for large discrete ill-posed problems", *J. Comput. Appl. Math.* **123** (2000) 423–446; doi:10.1016/S0377-0427(00)00414-3.
[7] K. L. Elmore and M. B. Richman, "Euclidean distance as a similarity metric for principal component analysis", *Mon. Weather Rev.* **129** (2001) 540–549; doi:10.1175/1520-0493(2001)129<0540:EDAASM>2.0.CO;2.
[8] P. T. Fletcher, "Geodesic regression and the theory of least squares on Riemannian manifolds", *Int. J. Comput. Vis.* **105** (2013) 171–185; doi:10.1007/s11263-012-0591-y.
[9] C. A. Glasbey and K. V. Mardia, "A review of image-warping methods", *J. Appl. Stat.* **25** (1998) 155–171; doi:10.1080/02664769823151.
[10] A. A. Goshtasby, *Image registration principles, tools and methods* (Springer, London, 2012); doi:10.1007/978-1-4471-2458-0.
[11] S. J. Greenfield, "Cauchy–Riemann equations in several variables", *Ann. Sc. Norm. Super. Pisa Cl. Sci.* **22** (1968) 275–314, available at https://eudml.org/doc/83459.
[12] U. Grenander and M. I. Miller, "Computational anatomy: an emerging discipline", *Q. Appl. Math.* **56** (1998) 617–694; doi:10.1090/qam/1668732.
[13] C. W. Groetsch, *The theory of Tikhonov regularization for Fredholm equations of the first kind*, (Pitman, London, 1984), available at https://www.researchgate.net/publication/233814596_The_theory_of_Tikhonov_regularization_for_Fredholm_equations_of_the_first_kind.
[14] H. Hsiao, C. Hsieh, X. Chen, Y. Gong, X. Luo and G. Liao, "New development of nonrigid registration", *ANZIAM J.* **55** (2014) 289–297; doi:10.1017/S1446181114000091.
[15] S. C. Joshi and M. I. Miller, "Landmark matching via large deformation diffeomorphisms", *IEEE Trans. Image Process.* **9** (2000) 1357–1370; doi:10.1109/83.855431.
[16] H. B. Keller, "Lectures on numerical methods in bifurcation problems", *Appl. Math.* **217** (1987) 50, available at https://www.math.tifr.res.in/~publ/ln/tifr79.pdf.
[17] S. Marsland and R. McLachlan, "A Hamiltonian particle method for diffeomorphic image registration", in: *Biennial international conference on information processing in medical imaging*, (Springer, Berlin, 2007) 396–407; doi:10.1007/978-3-540-73273-0_33.
[18] S. Marsland and C. J. Twining, "Clamped-plate splines and the optimal flow of bounded diffeomorphisms", in: *Statistics of large datasets, proceedings of Leeds annual statistical research workshop*, (University of Leeds, Leeds, 2002) 91–95, available at https://citeseerx.ist.psu.edu/viewdoc/download?doi=10.1.1.18.5291rep=rep1type=pdf.
[19] R. McLachlan and S. Marsland, "Discrete mechanics and optimal control for image registration", *ANZIAM J.* **48** (2007) 1–16; doi:10.21914/anziamj.v48i0.82.
[20] M. I. Miller, A. Trouvé and L. Younes, "Hamiltonian systems and optimal control in computational anatomy: 100 years since D'Arcy Thompson", *Annu. Rev. Biomed. Eng.* **17** (2015) 447–509; doi:10.1146/annurev-bioeng-071114-040601.
[21] J. Modersitzki, *Numerical methods for image registration*, (Oxford University Press, Oxford, 2004); doi:10.1093/acprof:oso/9780198528418.001.0001.
[22] X. Pennec, "Intrinsic statistics on Riemannian manifolds: Basic tools for geometric measurements", *J. Math Imaging Vis.* **25** (2006) 127; doi:10.1007/s10851-006-6228-4.
[23] S. V. Petukhov, "Non-Euclidean geometries and algorithms of living bodies", *Comput. Math. Appl.* **17** (1989) 505–534; doi:10.1016/0898-1221(89)90248-4.
[24] S. Saxena and R. K. Singh, "A survey of recent and classical image registration methods", *Int. J. Signal Process. Image Process. Pattern Recognit.* **7** (2014) 167–176; doi:10.14257/ijsip.2014.7.4.16.
[25] S. Sommer, F. Lauze, S. Hauberg and M. Nielsen, "Manifold valued statistics, exact principal geodesic analysis and the effect of linear approximations", in: *European conference on computer vision*, (Springer, Berlin, 2010) 43–56; doi:10.1007/978-3-642-15567-3_4.

[26] D. W. Thompson, *On growth and form*, (Cambridge University Press, Cambridge, 1942); doi:10.5962/bhl.title.6462.
[27] M. Y. Tufail, "*Image registration under conformal diffeomorphisms*", Ph. D. Thesis, Massey University, 2017, available at https://mro.massey.ac.nz/handle/10179/12459.
[28] J. R. Wells, "The Cauchy–Riemann equations and differential geometry", *Bull. Am. Math. Soc.* **6** (1982) 187–199; doi:10.1090/s0273-0979-1982-14976-x.
[29] L. Younes, *Shapes and diffeomorphisms*, (Springer, Berlin, 2010); doi:10.1007/978-3-642-12055-8.